

Received:
13 March 2018
Revised:
18 May 2018
Accepted:
25 June 2018

Cite as: Ramon Guirado,
Héctor Carceller,
Esther Castillo-Gómez,
Eero Castrén,
Juan Nacher. Automated
analysis of images for
molecular quantification in
immunohistochemistry.
Heliyon 4 (2018) e00669.
doi: [10.1016/j.heliyon.2018.e00669](https://doi.org/10.1016/j.heliyon.2018.e00669)



Automated analysis of images for molecular quantification in immunohistochemistry

Ramon Guirado^{a,*}, Héctor Carceller^a, Esther Castillo-Gómez^b, Eero Castrén^c,
Juan Nacher^{a,d}

^a Neurobiology Unit, Department of Cell Biology, Interdisciplinary Research Structure for Biotechnology and Biomedicine (BIOTECMED), Universitat de Valencia, Spain

^b Department of Medicine, School of Medical Sciences, Universitat Jaume I, Spain

^c Neuroscience Center, University of Helsinki, Finland

^d CIBERSAM: Spanish National Network for Research in Mental Health, Spain

* Corresponding author.

E-mail address: ramon.guirado@uv.es (R. Guirado).

Abstract

The quantification of the expression of different molecules is a key question in both basic and applied sciences. While protein quantification through molecular techniques leads to the loss of spatial information and resolution, immunohistochemistry is usually associated with time-consuming image analysis and human bias. In addition, the scarce automatic software analysis is often proprietary and expensive and relies on a fixed threshold binarization. Here we describe and share a set of macros ready for automated fluorescence analysis of large batches of fixed tissue samples using FIJI/ImageJ. The quantification of the molecules of interest are based on an automatic threshold analysis of immunofluorescence images to automatically identify the top brightest structures of each image. These macros measure several parameters commonly quantified in basic neuroscience research, such as neuropil density and fluorescence intensity of synaptic puncta, perisomatic innervation and col-localization of different molecules and analysis of the neurochemical phenotype of neuronal subpopulations. In addition, these same macro functions can be easily modified

to improve similar analysis of fluorescent probes in human biopsies for diagnostic purposes based on the expression patterns of several molecules.

Keywords: Neuroscience, Bioinformatics

1. Introduction

In clinical and biomedical studies, including both basic and applied neuroscience, one of the most relevant parts is the analysis of the expression levels of a given molecule. A precise and unbiased quantification is essential in order to understand how and where an experimental treatment or a disease is affecting the molecule of interest. Nowadays, the two main methods to get this information are either measurement in fresh tissue by molecular techniques or the quantification in fixed tissue by immunohistochemistry.

On one hand molecular techniques such as western blot or ELISA rely on multiple factors hard to standardize as the precision of the microdissection, which can cause inconsistent results in similar experiments (Ghosh et al., 2014). Moreover, the tissue lysing produces the loss of spatial and morphological information. On the other hand, the analysis of fixed tissue by immunohistochemistry can be easily standardized and allows to discriminate adjoining areas for a more accurate spatial analysis. Although immunohistochemistry has been criticized for non-linear correlation between protein expression and color detection (McCormick et al., 1993), more recent research has shown good linearity at the appropriate dynamic range (McCabe et al., 2005). Furthermore, several studies have correlated the results from immunostaining and protein levels with both western blot (Dias et al., 2000; Podhajsky et al., 1997) and ELISA (Simone et al., 2000). Consequently, immunohistochemistry has been extensively used for protein quantification in both basic research (Cordero et al., 2005; Varea et al., 2007) and diagnosis in clinical pathology (Seidal et al., 2001).

Despite the advantages of immunohistochemistry, the classic methodology employing 3,3'-Diaminobenzidine (DAB) typically relies on manual counting and scoring of gray levels in stained sections (Allred et al., 1998) as most analysis on immunofluorescence images (Di Cristo et al., 2007), introducing a level of subjectivity in the analysis that can bias the results. Moreover, manual analysis is a very intensive and time-consuming task, which frequently discourages researchers from performing this type of analysis. Different computational methods have been developed recently for automatic quantification of immunohistochemical (IHC) images based on segmentation methods to detect specific profiles, such as watershed segmentation method (Yu et al., 2009) or automatic thresholding algorithms (Haralick and Shapiro, 1985), especially for cancer diagnosis in human samples (Irshad et al., 2017). Nevertheless, most of these still rely on DAB staining, and therefore are

inappropriate for multiplexed studies in which the patterns of expression of several molecules are used for diagnosis instead of that of a single molecule per slice.

For all these reasons, we have gathered pieces of ImageJ macro language from different open sources and together with its macro recorder option, developed a series of macros to use with FIJI (Rueden et al., 2017; Schindelin et al., 2012). These macros allow us to perform automated analysis of immunofluorescence multi-labelled samples, which allows multiple channel co-localization between different molecules in discrete structures. By using a segmentation method based on the brightest percentage of the image, allows a sensitive measure of not only profiles, but also the measure of the fluorescence intensity of those profiles. In addition, by using single confocal planes this methodology is more robust regarding thickness variations; and by avoiding specific small areas such as clogged blood or tissue abnormalities is also more robust to any other sub-optimal steps during fixation that might compromise the results.

This method provides a fast and accurate analysis of several proteins in a single slice, providing not only better profiling in human tissue samples for diagnosis, but also different types of basic research analysis, including the density of perisomatic innervation inputs of specific neuronal subpopulations, the expression of activity markers such as the Fos protein family within a specific cellular subpopulation or the colocalization between different synaptic markers, providing a valuable functional insight.

2. Material and methods

2.1. Animals and histological procedure

The described methodology has been used in rat and mice tissue from our laboratories, but the examples we are showing here belong to mice from previous experiments.

All animal experimentation was conducted in accordance with the Directive 2010/63/EU of the European Parliament and of the Council of 22 September 2010 on the protection of animals used for scientific purposes and was approved by the Committee on Bioethics of the Universitat de Valencia and by the County Administrative board of Southern Finland.

Three months old mice were transcardially perfused with a working solution of paraformaldehyde (PFA) 4% in phosphate buffer (PB) 0.1M. We recommend to use recently prepared PFA solution, and 1 to 6 hours of post-fixation in the same fixative if perfusion was sub-optimal.

Freezing of the tissue usually results in reduced quality of the structural properties of the tissue, therefore we recommend only to freeze if the number of animals is very

high (it is faster to use a freezing sliding microtome) or if very thin sections are required (30 microns or thinner; cryostats allow thinner sectioning of the brain). Otherwise, we recommend using a vibratome.

Free-floating 50 micron sections are easy to collect and to work with, avoiding any further damage and destruction of the tissue. After collecting the sections, it can always be stored in PB 0.1M or PBS with 0.02–0.05% sodium azide to avoid bacterial growth, until the immunohistochemistry protocol.

Sections were processed as follows: after washing with phosphate saline buffer (PBS), non-specific binding was blocked by treatment with 10% normal donkey serum (NDS; Abcys), 0.2% Triton-X100 (Sigma) in PBS for 1 hour. Sections were then incubated for 48 hours at 4° with different primary antibody cocktails diluted in PBS-0.2% Triton-X100 (see [Table 1](#)). After washing, sections were incubated for 2 hours at room temperature with different secondary antibody cocktails also diluted in PBS-0.2% Triton-X100. Finally, sections were washed in PB 0.1M, mounted on slides and coverslipped using fluorescence mounting medium (Dako).

In the present study we used only commercial antibodies whose specificity was proved by the provider. Additionally, when the antigen used for generating the primary antibody was available, we first co-incubated them in accordance with the immunohistochemical protocol in order to block the binding of these antibodies to the tissue antigens. The primary antibody against VGlut1 was pre-adsorbed with the peptide used for their generation by their commercial source (Millipore, Cat# AG208). The primary antibody against Syn was pre-adsorbed with a synaptophysin recombinant protein (Novus, Cat#H00006855-P01). The antibody against PSA-NCAM was co-incubated with alpha-2,8-sialic acid (Colominic acid, Sigma-Aldrich Cat#C5762). The performance of the immunohistochemical procedure using these blocked antibodies resulted in a total absence of immunostaining.

The anti-GAD6, CAMKII, FosB, Reelin and VGAT antibodies were included in the former JCN Antibody Database, now integrated in the Antibody Registry database: <http://antibodyregistry.org/> the antibodies on this list have been described and characterized adequately according to the strict guidelines of the journal, including appropriate controls.

2.2. Confocal analysis and quantification

Images were acquired using a confocal microscope (Leica TCS SPE): we obtained z-stacks from every layer, strata or region of interest covering the whole thickness of the tissue. As previously mentioned, all the acquisition parameters were kept the same at all times: including a pinhole of 1 AU, the laser intensity, the gain of the photomultiplier, the offset of the histogram, and the image magnification. After

Table 1. List of primary and secondary antibodies used in the study.

Primary antibodies					
Anti-	Abbreviation	Host	Isotype	Dilution	Company
Calcium/calmodulin dependent protein kinase II	CAMKII	Mouse	Monoclonal IgG1	1:500	Abcam
glutamic acid decarboxylase 65/67	GAD65/67	Mouse	Monoclonal IgG	1:500	DSHB
FosB	FosB	Rabbit	Polyclonal IgG	1:500	Santa Cruz
Polysialylated form of the Neural Cell Adhesion Molecule	PSA-NCAM	Mouse	Monoclonal IgM	1:700	DSHB
Parvalbumin	PV	Guinea Pig	Polyclonal	1:2000	Synaptic Systems
Reelin	Reelin	Mouse	Monoclonal IgG1	1:2000	Millipore
Synaptophysin	SYN	Rabbit	Polyclonal	1:1000	Millipore
Vesicular GABA Transporter	VGAT	Mouse	Monoclonal IgG	1:1000	Synaptic Systems
Vesicular Glutamate Transporter 1	VGLUT1	Guinea Pig	Polyclonal	1:2000	Millipore
Secondary antibodies					
Anti-		Host	Label	Dilution	Company
Guinea Pig IgG		Donkey	Alexa 555	1:400	Jackson
Guinea Pig IgG		Donkey	Alexa 488	1:400	Jackson
Mouse IgG1		Donkey	DyLight 549	1:400	Jackson
Mouse IgG		Donkey	DyLight 649	1:400	Jackson
Mouse IgG		Donkey	Alexa 555	1:400	Molecular 2Probes
Mouse IgM		Donkey	DyLight 549	1:400	Jackson
Rabbit IgG		Donkey	Alexa 647	1:400	Invitrogen

analyzing the expression of the molecules of interest, we selected a single plane at the depth where the antibody detection was optimal. This selection depended on each antibody: generally synaptic proteins, such as the vesicular glutamate transporter 1 or synaptophysin do not penetrate more than a few microns on the surface of the sections, while other molecules, such as FosB or calcium binding proteins penetrate easily throughout the tissue (see Fig. 1A and B).

2.3. ELISA comparison

As described in a previous experiment from our laboratory (Castillo-Gómez et al., 2017), in which we tested the effects of social isolation, 64 male mice were treated with MK-801 at P9, and then either housed in “isolation” or “social” rearing between P21 and P90. Half of these animals (32) were processed for molecular quantitative

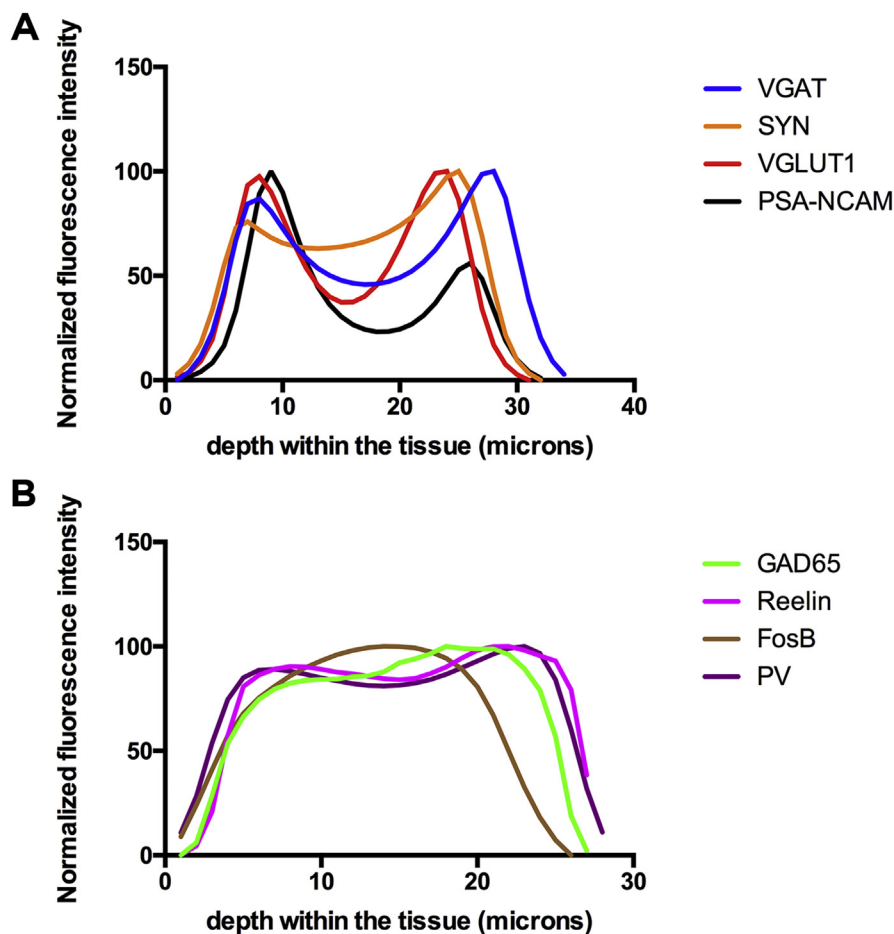


Fig. 1. Relationship between the fluorescence intensity (normalized values) and the depth within the tissue. A: Cross sectional profiles showing those molecules in which the detected signal is optimal at the surface of the sections. B: Cross sectional profiles showing those molecules in which the detected fluorescence intensity remains at optimal values through the section.

methods. In short, animals were decapitated at P90 and the amygdala dissected in fresh brain, then stored in liquid nitrogen and proteins were extracted to measure PSA-NCAM using an ELISA commercial kit (Eurobio/AbCys). The other half of the animals were transcardially perfused as indicated above for PSA-NCAM immunohistological processing. Then these values were compared using a t-test.

3. Results

We have designed an automatized protocol to analyze the expression of different molecules through antigen-antibody recognition in fixed tissue: the density of puncta expressing selected molecules in the neuropil, the puncta surrounding the somata of a specific neuronal subpopulation and the expression of different molecules in the somata of specific neuronal subpopulations.

3.1. Neuropil analysis

As previously discussed, one of the advantages of this technique is its high spatial resolution. Consequently, we can target any specific layer of the cortex or strata from the hippocampus, as in our example the stratum Lacunosum Moleculare by using a high magnification objective. The first step will be to convert the confocal images from the specific acquisition file (.lif in the case of Leica, .czi in Zeiss or .oif in Olympus confocals) to a format that can be read automatically by ImageJ/FIJI without the need of any plug-in, such as “.tiff”. For that we need to open all our images. In our case by using the bio-format importer included in FIJI, we can execute the “open all” option. Then, we can run a macro that will save all the opened images in.tiff within the selected folder (see macro 1 in the Supplementary material). Since we have acquired stacks from the whole section, we can easily select and export a specific z-step or projection of two or more consecutive z-steps (see macro 2; in line 9 we can define how many z-steps and at which depth in the stack to select) to carry out all the analysis within an optimal range of antibody detection. As commented above, the optimal depth is different for each antibody and we need to test the histogram for each molecule for optimal results (see Fig. 1).

Then, after making sure all the images are stored in the same folder (and that such folder contains exclusively image files), we can proceed to analyze these images, especially if we have already taken high magnification images. Alternatively, we can further zoom in to avoid factors potentially altering our data, such as non-uniform areas around somas, blood vessels or unspecific staining. Then, we can crop the area of interest, and save the resulting image as .tiff (keeping the metadata stored to work at the proper scale of image size). Other factors need to be taken into account to adjust to the specific spatial distribution of the detected molecule. For example, if we want to analyze the large giant boutons of the mossy fibers in the hippocampus or Tyrosine Hydroxylase (TH) fibers, we can modify the analyze particles command (macro 3: lines 35 and 66) to only analyze puncta of a specific size.

The main idea underlying this methodology is that all processing of the tissue has been, as much as possible, identical: same perfusion protocol, same incubation times, same laser intensity and acquisition settings such as the pinhole the gain and offset, to name a few. We use a macro that identifies a threshold separating the top % brightest part of the histogram from the rest, and therefore adjusting to the signal-to-noise ratio. Depending on the specific molecule to be analyzed, we use between 1 and 5%, but that can be easily adapted to other circumstances (see macro 3; in lines 15 and 46 we can select the percentage to be discarded after the binarization for each channel i.e. a value of 95 means we are selecting the top 5%).

Since the macro considers the signal-to-noise ratio of each image, its results are much more similar to manual analysis than a fixed threshold, with the advantage

of avoiding any human bias. Then, by running this macro, all the images contained in the selected folder will be processed (we usually analyze 3 images from different sections per region) and the total number and fluorescence intensity of the brightest puncta in each image will be calculated.

In short, this macro (see macro 3) activates a batch mode to analyze all the images contained within a specific folder (macro 3: lines 1 to 7), then it contains a Gaussian blur (macro 3: line 10), before splitting the different channels of the image to be analyzed separately (macro 3: line 11). The active image is identified as <id> and this way each channel is identified according to the order that it is opened by the software, being <id+1> the active image after closing <id> and so on (see line 13 to change to a particular channel). By duplicating the image at this point we will be able to measure the fluorescence intensity of the binarized mask, after the density of puncta is analyzed. Then it detects the threshold value to binarize at the indicated % of the histogram (macro 3: lines 15 to 28). It creates a binary mask representing the expression profile of that molecule (macro 3: line 30). Then, the number of profiles detected is analyzed (macro 3: line 35) in this mask and copied to the duplicate in order to measure the fluorescence intensity (macro 3: lines 36 to 42), and the process is repeated for any other channel we are interested to measure (line 44 we select <id+2>; see Fig. 2).

To assess the replicability and validity of our analysis, we compared our macro analysis and the molecular quantification method ELISA in two large sets of animals with the exact same experimental conditions. We could find significant differences between the animals reared in postweaning social isolation and those reared socially in both ELISA ($p < 0.01$) and our macro analysis of fluorescence intensity ($p = 0.02$; see Fig. 3A). Furthermore, we compared two binarization methods: fixed threshold and top brightest percentage. Manual counting resembles more the top brightest

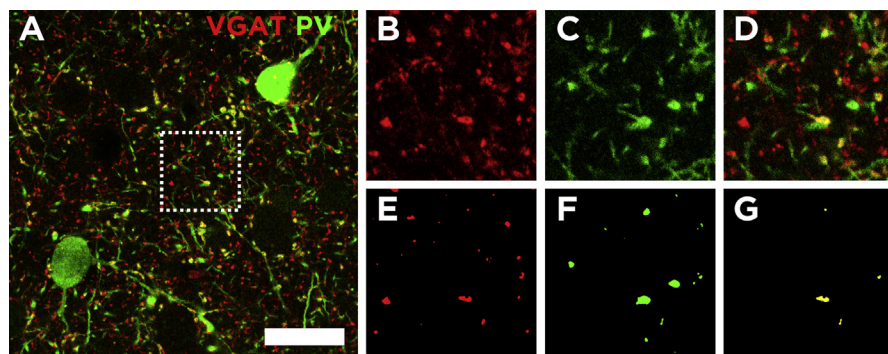


Fig. 2. Quantification of immunoreactive puncta in the neuropil expressing different molecules. A: Single confocal plane of a double labeled section showing the expression of VGAT and PV. B–E: Confocal planes of the area inside the dotted square in A, showing the original image (B to D) and the processed mask (E to G) for the puncta analysis for VGAT (B and E), and PV (C and F) and their co-localization (D and G). Scale bar: 20 μm in A, 9 μm in the insets.

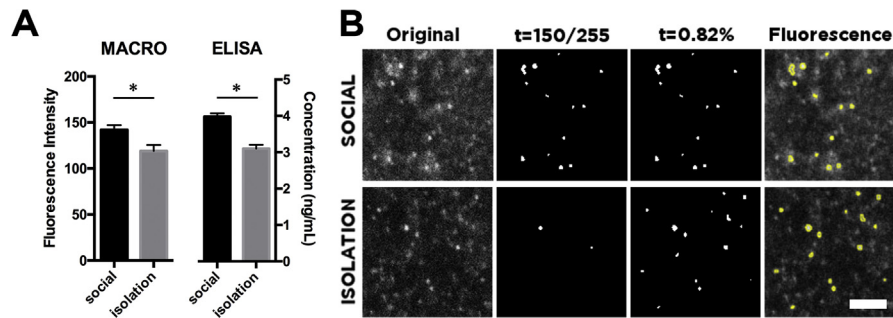


Fig. 3. Validation of the macro analysis. A: Histograms showing the comparison of PSA-NCAM expression with both our macro methodology and ELISA detection in animals subjected to the exact same experimental conditions. B: Single confocal planes from both animal groups binarized with a fixed threshold value, and with a top brightest percentage. Importantly, our macros allow provide both the total number of profiles found in the image and the fluorescence intensity within those profiles. Scale bar: 3 μ m.

approach, and it allows both: detection of changes in total number of neuropil elements and the analysis of the fluorescence within those profiles (see Fig. 3B).

3.2. Analysis of perisomatic puncta

Another interesting parameter that can be analyzed with the macro described above is the density of immunoreactive puncta surrounding the somata of certain neuronal subpopulations (see Fig. 4). The fluorescence detection of different markers such as CAMKII, GluR2/3, PV or a fluorescent reporter such as GFP or TdTomato, can be used to identify the perimeter of the soma of specific neuronal subpopulations. We can manually delineate this perimeter on ImageJ/FIJI in single z-steps (obtained as described previously running macro 2). Then we will open a

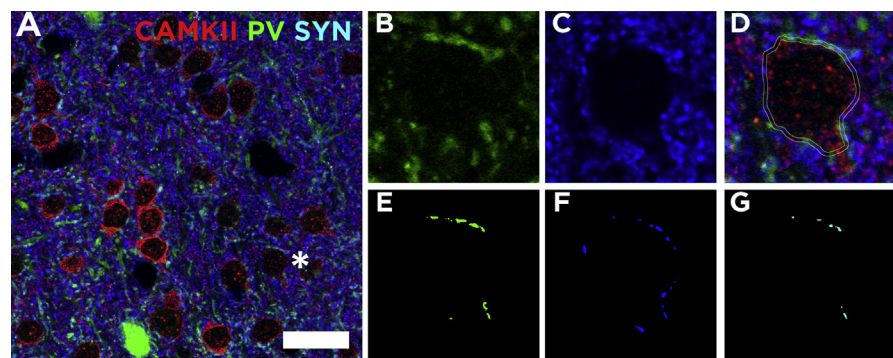


Fig. 4. Quantification of the perisomatic puncta surrounding a pyramidal cell in the mouse neocortex. A: Single confocal plane showing the expression of the CAMKII, PV and SYN. The asterisk indicates the pyramidal cell used as example. B–G: focal planes showing the original image and processed mask for analysis of the PV (B and E), SYN (C and F). D: composite image and the area between the somatic profile and a selection enlargement of 0.5 μ m where the analysis of the processed masks is carried out (G). Scale bar: 28 μ m in A, 8 μ m in the insets.

new macro (see macro 4) that we run after manually delineating the perimeter of a given cell. The macro will mark that selection to a ROI manager (macro 4: lines 2 to 4). Then, the macro will measure the perimeter of the delineated profile (first of the measurements results), needed to calculate the perisomatic innervation density (macro 4: line 5). Then, the macro will make a new expanded selection of a specific thickness (we use values between 0.5 to 1 micron thick; macro 4: line 6). Subsequently, the macro will duplicate a specific channel to provide both the total number of puncta as previously described (macro 4: lines 16 to 40) and the fluorescence intensity of those puncta (macro 4: lines 42 to 44). This process can be repeated with as many channels as our images contain. For a workflow showing the different steps with a sample image see Fig. 5.

In total this macro returns three measures within the measurements dialogue box: the first line corresponds to the perimeter of the soma, the second line to the intensity of the channel 2 of our image—in our case SYN- and the third line to the intensity of the puncta analyzed for the channel 3—PV in our example-. In addition it returns three results from the analyze particles summary dialogue box, which correspond to total number of puncta binarized for channel 2, channel 3 and the colocalization of both, respectively.

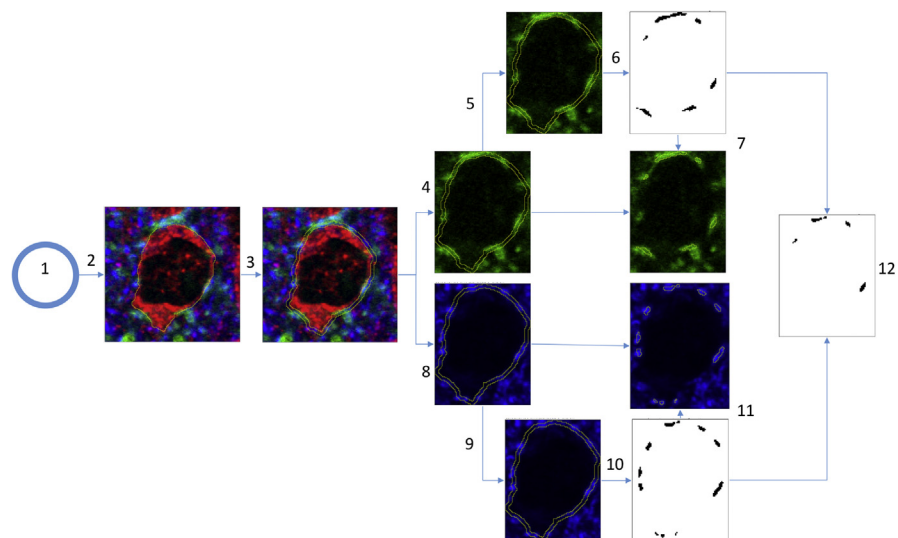


Fig. 5. Workflow diagram representing different steps of macro processing. 1: initial conditions are established: set scale, set measurements options, etc. 2: the manually drawn profile of a neuron is added to the ROI manager. 3: The selection is enlarged and a XOR option defines the perisomatic region (i.e., the area between the original selection and the enlarged selection). 4 and 5: The green channel only is duplicated two times. 6: in one of these two copies is processed by a Gaussian blur and a clear outside options, to threshold high intensity pixels, creating a mask, that is analyzed to obtain the number of puncta expressing the green fluorophore. 7: This mask is restored to the original duplicate to measure the fluorescence intensity within the mask. 8–11: the same process is repeated on the blue channel. 12: The colocalization between both masks is calculated through the AND option, and the result is analyzed, providing the number of puncta co-expressing the green and the blue fluorophores.

3.3. Analysis of neuronal somata

Finally, our macros can also be applied to analyze the expression of activity-related molecules such as c-fos, arc or FosB within a specific neuronal subpopulation (see Fig. 6). Since here we are interested in the fluorescence intensity within a specific mask, we can use the method described in previous macros for binarization of the top 1% or 5% directly to create a mask that can be copied (macro 5: lines 33 and 34) and applied to the channel containing the activity marker to measure the fluorescence intensity within that mask (macro 5: lines 40 to 42). In this way, this macro will automatically identify the profiles of that specific subpopulation expressing molecules such as GFP, CAMKII or PV to create a mask (see Fig. 6E) to be applied on the channel of our molecule of interest and analyze the fluorescence intensity within those profiles (see Fig. 6F).

4. Discussion

We have described here a series of macros for ImageJ/FIJI image analysis. These macros provide a fast and accurate automatic method to improve the replicability of histological analysis, reduce the time usually required for this type of image analysis and eliminate any human related bias from the analysis.

Automatized methodologies for quantification of the protein expression levels have been developed recently thanks to the refinement of image processing software.

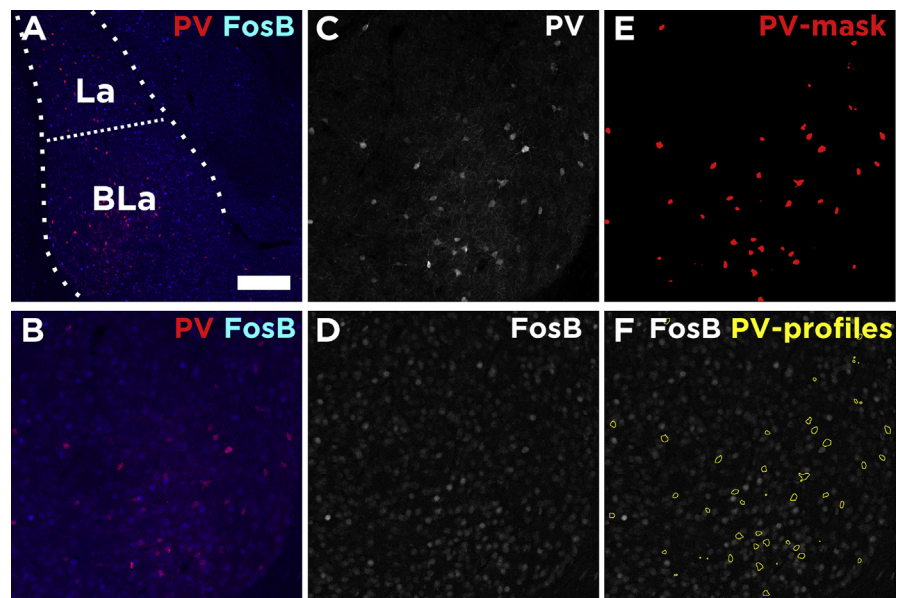


Fig. 6. Quantification of somatic colocalization in the mouse amygdala. A: Low magnification image of the amygdala showing PV and FosB distribution. B: Single confocal plane of the area analyzed in the basolateral amygdala. C and D: confocal planes showing the original split images of the PV and FosB respectively. E: confocal planes showing the processed mask of PV expression. F: Focal plane showing both the FosB expression and in yellow the profiles of PV interneurons. Scale bar: 200 μm in A, 100 μm in the others.

These methodologies have been especially used in clinical pathology of different diseases, including cancer and Alzheimer disease (Varghese et al., 2014). Most of these methods perform automatic analysis on DAB stained sections of a given pathological marker (Huang et al., 1996; Matkowskyj et al., 2000; Underwood et al., 2001).

Nevertheless, in neuroscience and other basic sciences using microscopic analysis, the use of at least two different markers is very common, and allows to study their correlation, colocalization and/or other characteristics of interest regarding their spatial distribution. As shown above, fluorescent immunolabeling allows the detection of several molecules in a single section without losing spatial information and provides functional insight thanks to that spatial relationship. Examples of this relationship are the detection of certain molecules expressed in the nucleus within a specific calcium binding protein neuronal subpopulation (Antila et al., 2017), the detection of synaptic proteins in overlap with an inhibitory or excitatory neurotransmitter transporter (Guirado et al., 2012; Sánchez-Huertas and Rico, 2011) or the study of the perisomatic innervation of certain subpopulations of neurons (Favuzzi et al., 2017; Fazzari et al., 2010; Guirado et al., 2014; Kobayashi et al., 2010). On the other hand, in clinical studies immunofluorescence imaging is delivering more promising results regarding multiplexing: studying expression levels of protein clusters from a single sample (Alonso et al., 2004; Makretsov et al., 2004), suggesting our macros could be used in the clinic for a better diagnosis in human samples as well.

Nevertheless, most methodologies are based on the selection of an optimal threshold previously selected from the tissue analyzed. The criteria of choosing a specific fixed threshold is a current problem that produces variable results, since different sections might have different quality of fixation and, as a consequence, there is no an optimal single threshold for a batch of images (Choudhury et al., 2010). In contrast, our macros are not based on this manual threshold selection. They detect the optimal threshold by detecting the indicated top % of brightest elements on the image, as others have used similarly before (Fedorov et al., 2009). This automated selection of the threshold allows the macros to adapt to small alterations in the tissue staining, reducing the variability induced by applying a harsh threshold manually configured. Moreover, we provide the code of the macros used (see supplementary material) and indications of how to change key elements, encouraging other researchers to adapt them to their specific needs.

Declarations

Author contribution statement

Ramon Guirado: Conceived and designed the experiments; Performed the experiments; Analyzed and interpreted the data; Wrote the paper.

Héctor Carceller, Esther Castillo-Gómez: Performed the experiments.

Eero Castrén, Juan Nacher: Contributed reagents, materials, analysis tools or data; Wrote the paper.

Funding statement

This work was supported by the extinct Spanish Ministry of Science (#BES, 2007–15757), the ERC Advanced grant (#322742-iPlasticity), the Academy of Finland (#257486), the Spanish Ministry of Economy and Competitiveness (SAF2015-68436-R) and the Juan de la Cierva program (IJCI-2016-27758).

Competing interest statement

The authors declare no conflict of interest.

Additional information

Supplementary content related to this article has been published online at <https://doi.org/10.1016/j.heliyon.2018.e00669>.

References

- Allred, D.C., Harvey, J.M., Berardo, M., Clark, G.M., 1998. Prognostic and predictive factors in breast cancer by immunohistochemical analysis. *Mod. Pathol.* 11, 155–168.
- Alonso, S.R., Ortiz, P., Pollán, M., Pérez-Gómez, B., Sánchez, L., Acuña, M.J., Pajares, R., Martínez-Tello, F.J., Hortelano, C.M., Piris, M.A., Rodríguez-Peralto, J.L., 2004. Progression in cutaneous malignant melanoma is associated with distinct expression profiles: a tissue microarray-based study. *Am. J. Pathol.* 164, 193–203.
- Antila, H., Ryazantseva, M., Popova, D., Sipilä, P., Guirado, R., Kohtala, S., Yalcin, I., Lindholm, J., Vesa, L., Sato, V., Cordeira, J., Autio, H., Kislin, M., Rios, M., Joca, S., Casarotto, P., Khiroug, L., Lauri, S., Taira, T., Castrén, E., Rantamäki, T., 2017. Isoflurane produces antidepressant effects and induces TrkB signaling in rodents. *Sci. Rep.*
- Castillo-Gómez, E., Perez-Rando, M., Bellés, M., Gilabert-Juan, J., Llorens, J.V., Carceller, H., Bueno-Fernández, C., García-Mompó, C., Ripoll-Martínez, B., Curto, Y., Sebastiá-Ortega, N., Moltó, M.D., Sanjuan, J., Juan, N., 2017. Early social isolation stress and perinatal NMDA receptor antagonist treatment induce changes in the structure and neurochemistry of inhibitory neurons of the adult amygdala and prefrontal cortex. *Eneuro* 4, ENEURO.0034–17.2017.

- Choudhury, K.R., Yagle, K.J., Swanson, P.E., Krohn, K.A., Rajendran, J.G., 2010. A robust automated measure of average antibody staining in immunohistochemistry images. *J. Histochem. Cytochem.* 58, 95–107.
- Cordero, M.I., Rodríguez, J.J., Davies, H.A., Peddie, C.J., Sandi, C., Stewart, M.G., 2005. Chronic restraint stress down-regulates amygdaloid expression of polysialylated neural cell adhesion molecule. *Neuroscience* 133, 903–910.
- Di Cristo, G., Chattopadhyaya, B., Kuhlman, S.J., Fu, Y., Bélanger, M.-C., Wu, C.Z., Rutishauser, U., Maffei, L., Huang, Z.J., 2007. Activity-dependent PSA expression regulates inhibitory maturation and onset of critical period plasticity. *Nat. Neurosci.* 10, 1569–1577.
- Dias, P., Chen, B., Dilday, B., Palmer, H., Hosoi, H., Singh, S., Wu, C., Li, X., Thompson, J., Parham, D., Qualman, S., Houghton, P., 2000. Strong immunostaining for myogenin in rhabdomyosarcoma is significantly associated with tumors of the alveolar subclass. *Am. J. Pathol.* 156, 399–408.
- Favuzzi, E., Marques-Smith, A., Deogracias, R., Winterflood, C.M., Sánchez-Aguilera, A., Mantoan, L., Maeso, P., Fernandes, C., Ewers, H., Rico, B., 2017. Activity-dependent gating of parvalbumin interneuron function by the perineuronal net protein Brevican. *Neuron* 95, 639–655.e10.
- Fazzari, P., Paternain, A.V., Valiente, M., Pla, R., Luján, R., Lloyd, K., Lerma, J., Marín, O., Rico, B., 2010. Control of cortical GABA circuitry development by Nrg1 and {ErbB4} signalling. *Nature* 464, 1376–1380.
- Fedorov, V.V., Schuessler, R.B., Hemphill, M., Ambrosi, C.M., Chang, R., Voloshina, A.S., Brown, K., Hucker, W.J., Efimov, I.R., 2009. Structural and functional evidence for discrete exit pathways that connect the canine sinoatrial node and atria. *Circ. Res.* 104, 915–923.
- Ghosh, R., Gilda, J.E., Gomes, A.V., 2014. The necessity of and strategies for improving confidence in the accuracy of western blots. *Expert Rev. Proteom.* 11, 549–560.
- Guirado, R., Perez-Rando, M., Sanchez-Matarredona, D., Castrén, E., Nacher, J., 2014. Chronic fluoxetine treatment alters the structure, connectivity and plasticity of cortical interneurons. *Int. J. Neuropsychopharmacol.* 17.
- Guirado, R., Sanchez-Matarredona, D., Varea, E., Crespo, C., Blasco-Ibáñez, J.M., Nacher, J., 2012. Chronic fluoxetine treatment in middle-aged rats induces changes in the expression of plasticity-related molecules and in neurogenesis. *BMC Neurosci.* 13, 5.

Haralick, R.M., Shapiro, L.G., 1985. Image segmentation techniques. *Comput. Vision Graph. Image Process.* 29, 100–132.

Huang, X., Chen, S., Tietz, E.L., 1996. Immunocytochemical detection of regional protein changes in rat brain sections using computer-assisted image analysis. *J. Histochem. Cytochem.* 44, 981–987.

Irshad, H., Oh, E.-Y., Schmolze, D., Quintana, L.M., Collins, L., Tamimi, R.M., Beck, A.H., 2017. Crowdsourcing scoring of immunohistochemistry images: evaluating performance of the crowd and an automated computational method. *Sci. Rep.* 7, 43286.

Kobayashi, K., Ikeda, Y., Sakai, A., Yamasaki, N., Haneda, E., Miyakawa, T., Suzuki, H., 2010. Reversal of hippocampal neuronal maturation by serotonergic antidepressants. *Proc. Natl. Acad. Sci. U. S. A.* 107, 8434–8439.

Makretsov, N.A., Huntsman, D.G., Nielsen, T.O., Yorida, E., Peacock, M., Cheang, M.C.U., Dunn, S.E., Hayes, M., van de Rijn, M., Bajdik, C., Gilks, C.B., 2004. Hierarchical clustering analysis of tissue microarray immunostaining data identifies prognostically significant groups of breast carcinoma. *Clin. Cancer Res.* 10, 6143–6151.

Matkowskyj, K.A., Schonfeld, D., Benya, R.V., 2000. Quantitative immunohistochemistry by measuring cumulative signal strength using commercially available software Photoshop and Matlab. *J. Histochem. Cytochem.* 48, 303–311.

McCabe, A., Dolled-Filhart, M., Camp, R.L., Rimm, D.L., 2005. Automated quantitative analysis (AQUA) of in situ protein expression, antibody concentration, and prognosis. *J. Natl. Cancer Inst.* 97, 1808–1815.

McCormick, D., Yu, C., Hobbs, C., Hall, P.A., 1993. The relevance of antibody concentration to the immunohistological quantification of cell proliferation-associated antigens. *Histopathology* 22, 543–547.

Podhajsky, R.J., Bidanset, D.J., Caterson, B., Blight, A.R., 1997. A quantitative immunohistochemical study of the cellular response to crush injury in optic nerve. *Exp. Neurol.* 143, 153–161.

Rueden, C.T., Schindelin, J., Hiner, M.C., DeZonia, B.E., Walter, A.E., Arena, E.T., Eliceiri, K.W., 2017. ImageJ2: ImageJ for the next generation of scientific image data. *BMC Bioinf.* 18, 529.

Sánchez-Huertas, C., Rico, B., 2011. CREB-dependent regulation of GAD65 transcription by BDNF/TrkB in cortical interneurons. *Cereb. Cortex* 21, 777–788.

Schindelin, J., Arganda-Carreras, I., Frise, E., Kaynig, V., Longair, M., Pietzsch, T., Preibisch, S., Rueden, C., Saalfeld, S., Schmid, B., Tinevez, J.-Y., White, D.J.,

Hartenstein, V., Eliceiri, K., Tomancak, P., Cardona, A., 2012. Fiji: an open-source platform for biological-image analysis. *Nat. Methods* 9, 676–682.

Seidal, T., Balaton, A.J., Battifora, H., 2001. Interpretation and quantification of immunostains. *Am. J. Surg. Pathol.* 25, 1204–1207.

Simone, N.L., Remaley, A.T., Charboneau, L., Petricoin, E.F., Glickman, J.W., Emmert-Buck, M.R., Fleisher, T.A., Liotta, L.A., 2000. Sensitive immunoassay of tissue cell proteins procured by laser capture microdissection. *Am. J. Pathol.* 156, 445–452.

Underwood, R.A., Gibran, N.S., Muffley, L.A., Usui, M.L., Olerud, J.E., 2001. Color subtractive—computer-assisted image analysis for quantification of cutaneous nerves in a diabetic mouse model. *J. Histochem. Cytochem.* 49, 1285–1291.

Varea, E., Blasco-Ibáñez, J.M., Gómez-Climent, M.Á., Castillo-Gómez, E., Crespo, C., Martínez-Guijarro, F.J., Nácher, J., 2007. Chronic fluoxetine treatment increases the expression of PSA-NCAM in the medial prefrontal cortex. *Neuropsychopharmacology* 32, 803–812.

Varghese, F., Bukhari, A.B., Malhotra, R., De, A., 2014. IHC profiler: an open source plugin for the quantitative evaluation and automated scoring of immunohistochemistry images of human tissue samples. *PLoS One* 9, e96801.

Yu, W., Lee, H.K., Hariharan, S., Bu, W., Ahmed, S., 2009. Quantitative neurite outgrowth measurement based on image segmentation with topological dependence. *Cytometry A* 75, 289–297.